Simulation study of ICRF wave propagation and absorption in 3-D magnetic configurations

T. Yamamoto[1)], S. Murakami[1)] and A. Fukuyama[1)]

[1)]*Department of Nuclear Engineering, Kyoto University, Kyoto 606-8501, Japan*

(Received 15 October 2007)

ICRF wave propagation and absorption are investigated by TASK/WM, in which Maxwell's equation for RF wave electric field with complex frequency is solved as a boundary value problem in 3D magnetic configurations. Magnetic flux coordinates based on the MHD equilibrium by VMEC code are considered. The wave propagation is solved in the tokamak configuration (JT-60U) and also in the helical configuration (LHD) in the minority ion heating regime. Characteristics of the ICRF wave propagation and absorbed in the 3D magnetic configurations are shown.

Keywords: Simulation, ICRF heating, wave propagation, helical configuration

1 Introduction

The ICRF heating has been successfully studied and the efficiency of this heating method has been shown in LHD. The numerical analysis of ICRF heating has been carryed out by GNET[1] and also have shown the efficiency and detail information about the energetic tail ion distribution generated by ICRF heating. However, a detail analysis of the wave propagation and absorption process has not been carryed out enough in 3D magnetic configurations.

In this paper we study the ICRF wave propagation and absorption by TASK/WM[2, 3], in which Maxwell's equation for RF wave electric field with complex frequency is solved as a boundary value problem in 3D magnetic configurations. We consider VMEC coordinate as the magnetic coordinate obtained from MHD equilibrium. We first solve the wave propagation in the tokamak configuration (JT-60U) and , then, the propagation in the helical configuration (LHD), where the minority ion heating regime is assumed.

2 Simulation model

TASK/WM solves Maxwell's equation for the electric field $\mathbf{E}$ with complex frequency ω as a boundary value problem in 3D magnetic configurations.

$$\nabla \times \nabla \times \mathbf{E} = \frac{\omega^2}{c^2} \overset{\leftrightarrow}{\epsilon} \cdot \mathbf{E} + i\omega\mu_0 \mathbf{j}_{\rm ext} \tag{1}$$

Here, the external current $\mathbf{j}_{\rm ext}$ represents the antenna current in ICRF heating. Assuming cold plasma and collisional dumping, the dielectric tensor is

$$\begin{aligned}
\overset{\leftrightarrow}{\epsilon} &= \begin{pmatrix} S & -iD & 0 \\ iD & S & 0 \\ 0 & 0 & P \end{pmatrix}, \\
S &= 1 - \frac{1}{\epsilon_0}\sum_s \frac{\omega_{\rm ps}^2}{\omega}\frac{\omega + i\nu_s}{(\omega + i\nu_s)^2 - \Omega_s^2}, \\
D &= \frac{1}{\epsilon_0}\sum_s \frac{\omega_{\rm ps}^2}{\omega}\frac{\Omega_s}{(\omega + i\nu_s)^2 - \Omega_s^2}, \\
P &= 1 - \sum_s \frac{\omega_{\rm ps}^2}{\omega}\frac{1}{\omega + i\nu_s},
\end{aligned} \tag{2}$$

where particle species s, the dielectric constant in vacuum ϵ_0, the collisionality ν, the plasma frequency $\omega_{\rm p}$ and the cyclotron frequency Ω.

We rewrite the Maxwell's equation (1) in a magnetic coordinates (ψ, θ, φ). LHS of (1) is written as

$$\begin{aligned}
&(\nabla \times \nabla \times \mathbf{E})^p \\
&= \frac{1}{J}\Bigg[\frac{\partial}{\partial x^q}\Bigg\{\frac{g_{rp}}{J}\left(\frac{\partial E_r}{\partial x^q} - \frac{\partial E_q}{\partial x^r}\right) + \frac{g_{rq}}{J}\left(\frac{\partial E_p}{\partial x^r} - \frac{\partial E_r}{\partial x^p}\right) \\
&\quad + \frac{g_{rr}}{J}\left(\frac{\partial E_q}{\partial x^p} - \frac{\partial E_p}{\partial x^q}\right)\Bigg\} - \frac{\partial}{\partial x^r}\Bigg\{\frac{g_{qp}}{J}\left(\frac{\partial E_r}{\partial x^q} - \frac{\partial E_q}{\partial x^r}\right) \\
&\quad + \frac{g_{qq}}{J}\left(\frac{\partial E_p}{\partial x^r} - \frac{\partial E_r}{\partial x^p}\right) + \frac{g_{qr}}{J}\left(\frac{\partial E_q}{\partial x^p} - \frac{\partial E_p}{\partial x^q}\right)\Bigg\}\Bigg],
\end{aligned} \tag{3}$$

where the metric coefficient $g_{ij} = \mathbf{e}_i \cdot \mathbf{e}_j$, $\mathbf{e}_i = \partial\mathbf{r}/\partial\mathbf{x}^{\mathbf{i}}$, Jacobian J, $(x^1, x^2, x^3) = (\psi, \theta, \varphi)$. The indexes (p, q, r) are $(1, 2, 3), (2, 3, 1), (3, 1, 2)$.

The dielectric tensor is written as

$$\tilde{\epsilon}_{ij} = \overset{\leftrightarrow}{g}{}^{-1}_{ij} \cdot \overset{\leftrightarrow}{\mu}_{ij} \cdot \overset{\leftrightarrow}{\epsilon}_{ij} \cdot \overset{\leftrightarrow}{\mu}{}^{-1}_{ij}, \tag{4}$$

author's e-mail: yamamoto@p-grp.nucleng.kyoto-u.ac.jp

where the rotation transform tensor $\overleftrightarrow{\mu}$ is

$$\begin{aligned}
\mu_{11} &= \frac{1}{\sqrt{g^{11}}}, \\
\mu_{12} &= \frac{1}{J\sqrt{g^{11}}}\left\{\frac{B^\theta}{B}(g_{23}g_{12}-g_{22}g_{31}) \right. \\
&\qquad \left. + \frac{B^\varphi}{B}(g_{33}g_{12}-g_{23}g_{31})\right\}, \\
\mu_{13} &= \frac{B^\theta}{B}g_{12} + \frac{B^\varphi}{B}g_{13}, \quad \mu_{21} = 0, \\
\mu_{22} &= \frac{B^\varphi}{B}J\sqrt{g^{11}}, \quad \mu_{23} = \frac{B^\theta}{B}g_{22} + \frac{B^\varphi}{B}g_{23}, \\
\mu_{31} &= 0, \quad \mu_{32} = -\frac{B^\theta}{B}J\sqrt{g^{11}}, \\
\mu_{33} &= \frac{B^\theta}{B}g_{32} + \frac{B^\varphi}{B}g_{33}. \qquad (5)
\end{aligned}$$

The electric field $\mathbf{E}$ and metric coefficient g_{ij} are evaluated at grid points ψ_l in radial direction and expanded to Fourier series in poloidal and toroidal direction.

$$\begin{aligned}
\mathbf{E}(\psi_k,\theta,\varphi) &= \sum_{mn}\mathbf{E}_{mn}(\psi_k)e^{i(m\theta+n\varphi)}, \\
g_{ij}(\psi_k,\theta,\varphi) &= \sum_{m'n'}(g_{ij})_{m'n'}(\psi_k)e^{i(m'\theta+n'N_h\varphi)}, \qquad (6)
\end{aligned}$$

where N_h is rotation number of helical coil in φ. The antenna current $\mathbf{j}_{\rm ext}$ is given as

$$\begin{aligned}
j^1 &= (j^1)_{mn}e^{i(m\theta+n\varphi)}\Theta(\psi_d-\psi), \\
j^{2,3} &= (j^{2,3})_{mn}e^{i(m\theta+n\varphi)}\delta(\psi-\psi_d), \qquad (7)
\end{aligned}$$

where step function $\Theta(x)$, delta function $\delta(x)$, and the radial antenna position ψ_d. These equations satisfy $\nabla\cdot\mathbf{j}_{\rm ext} = 0$.

We assume that the plasma is surrounded by a perfect conductor and that there is a vacuum layer between the plasma surface and the perfect conductor wall. Then, the tangential electric field at the wall is set zero as the boundary condition;

$$E_\theta^{mn} = 0, \quad E_\varphi^{mn} = 0. \qquad (8)$$

The poloidal electric field at the magnetic axis $\psi = 0$ is zero. The toroidal electric fields of the modes $m \neq 0$ are zero. That of mode $m = 0$ is finite and the radial derivation is zero. These are boundary condition on the magnetic axis $\psi = 0$;

$$\left\{\begin{array}{ll} m = 0 & \frac{\partial E_\varphi^{0n}}{\partial\psi} = 0 \\ m \neq 0 & E_\varphi^{mn} = 0. \end{array}\right. \qquad (9)$$

The Maxwell's equations (3)-(7) are solved under the boundary conditions (8) and (9) on the 3D configuration given by numerical equilibrium data of the magnetic flux coordinates.

3 Simulation results

3.1 Tokamak configuration (JT-60U)

We first study the ICRF minority heating in the tokamak configuration, taking JT-60U plasma as example. The assumed configuration parameters are as follows; plasma major radius $R_0 = 3.5$m, plasma minor radius $a = 0.98$m, plasma shape elongation $\kappa = 1.3$, plasma shape triangularity $\delta = 0.31$, magnetic field at magnetic axis $B_0 = 3.3$T.

The obtained results for the minority ion heating regime is showen in Fig.1. The assumed plasma parameters are as follows; temperature at magnetic axis $T_0 = 3.0$keV, temperature on plasma boundary $T_s = 0.3$keV, density at magnetic axis $n_0 = 1.0\times10^{20}/\mathrm{m}^3$, density on plasma boundary $n_s = 0.1\times10^{20}/\mathrm{m}^3$, minor ion ratio 5%, ration of collision frequency to wave frequency $\nu_s = 0.003$. The temperature and density profiles are given by $T(r/a) = (T_0-T_s)(1-(r/a)^2)+T_s$, $n(r/a) = (n_0-n_s)(1-(r/a)^2)^{1/2}+n_s$ respectively. Also, the used antenna parameters are antenna current density $j_{\rm ext} = 1.0$A/m, wave frequency $f_{RF} = 45.0$MHz, The upper side figures in Fig.1 assumes the wave frequency $f_{RF} = 45.0$MHz and the lower side figures is $f_{RF} = 48.0$MHz.

Three lines drawn in Fig.1 (b), (f) represent ion cyclotron layer (a green line), two-ion-hybrid cut-off (a blue line) and resonance (a red line) layers from the outside. It is observed that the absorption region of minority ion locates near the minority ion cyclotron layer in Fig.1 (b), (f). The coherent waves are observed (c), (d), (g), (h). The E_+ component (right-circularly polarized component) of the electric field is absorbed and the amplitude of coherent waves is damped near the minority ion cyclotron layer (c), (g). While, the damping of amplitude of the E_- component (left-circularly polarized component) not observed near the minority ion cyclotron layer. The reason is that the E_- component of the electric field do not provide the minority ion at the minority ion cyclotron layer under the assumption of cold plasma. The absorption increases at the two-ion-hybrid resonance and cut-off layers near the minority ion cyclotron layer near $z = 0$ (a), (b). Since the width between resonance and cut-off is narrow, the wave is reflected or transmitted at the cut-off layers. The reflected waves is superposed incoming waves and the amplitude of E_+ component is enhanced (c). The amplitude of the transmitted wave is enhanced at the resonance layer (c). These are the reasons for increasement of the absorption.

The lower in Fig.1 are results for the same parameters as those of upper except $f_{RF} = 48$MHz. Since the wave frequency increases from 45.0MHz to 48.0MHz, the ion cyclotron layer and the two-ion-hybrid cut-off and resonance layer shift toward the higher magnetic field side. Therefore, the absorption region moves from 4.0m (b) to 3.75m (f).

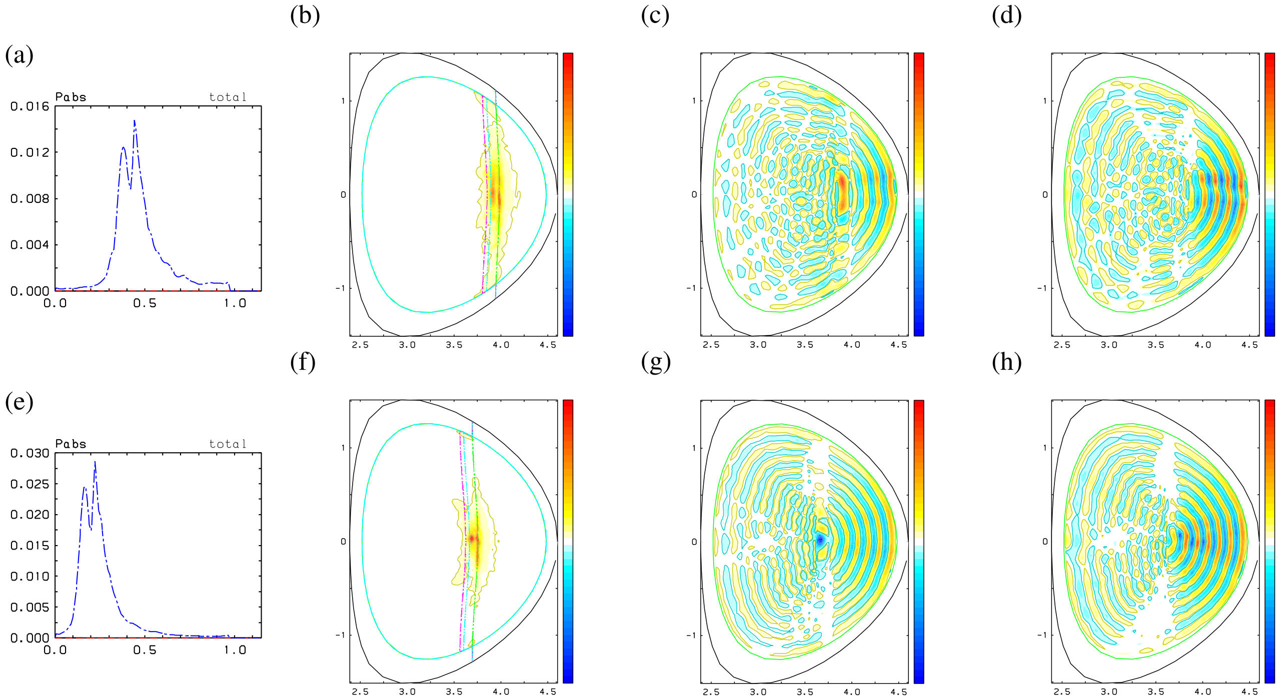

Fig. 1 Radial H absorption distributions (a), (e), contour plots of H absorption (b), (f) and E_+ component (c), (g) and E_- component (d), (h) of the electric field on the poloidal cross section; upper (f_{RF} = 45.0MHz), lower (f_{RF} = 48.0MHz); JT-60U

3.2 Helical configuration (LHD)

We study the ICRF minority heating in the Helical configuration, taking the LHD plasma as an example. The configuration parameters of LHD are as follows; plasma major radius R_0 = 3.6m, plasma minor radius a = 0.58m, magnetic field at magnetic axis B_0 = 2.75T.

The magnetic surface structure obtained by VMEC code is shown in Fig.2, where a vertically elongated cross section is plotted.

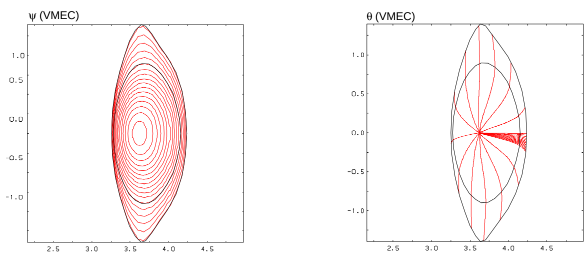

Fig. 2 Conter plots of a magnetic surface structure, ψ (left fig.), θ (right fig.)

The obtained results for the minority ion heating regime in the LHD plasma is showed in Fig.4. Upper side figures in Fig.4 are results with following plasma parameters; temperature at magnetic axis T_0 = 2.0keV, temperature on plasma boundary T_s = 0.2keV, density at magnetic axis $n_0 = 0.1 \times 10^{20}/\mathrm{m}^3$, density on plasma boundary $n_s = 0.01 \times 10^{20}/\mathrm{m}^3$, minority ion ratio 5%, ration of collision frequency to wave frequency ν_s = 0.003 . The used antenna parameters is antenna current density j_{ext} = 1.0A/m, wave frequency f_{RF} = 38.5MHz. Also, the temperature and density profile are given $T(r/a) = (T_0 - T_s)(1-(r/a)^2) + T_s$, $n(r/a) = (n_0 - n_s)(1-(r/a)^8) + n_s$ respectively. These parameters is used in an experiment on LHD.

The lower in Fig.4 are results used the same parameters as those of upper except $n_0 = 0.7 \times 10^{20}/\mathrm{m}^3$, f_{RF} = 36.0MHz, the center mode number of the toroidal wave mode number $nph0 = 0$; $n = nph0 + n'' N_h$, where n'' = integer (n in Eq.6), is the toroidal mode number of the waves exited by antenna current. The toroidal mode number dependency is showed in 3. It shows that $nph0 = 0$ is the leading mode number. Therefore, the lower in Fig.4 was analyzed with $nph0 = 0$.

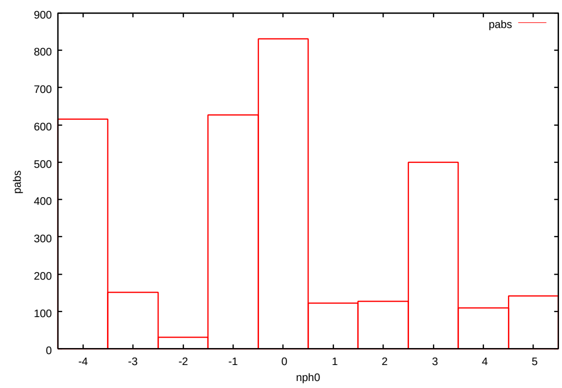

Fig. 3 Toroidal mode dependency

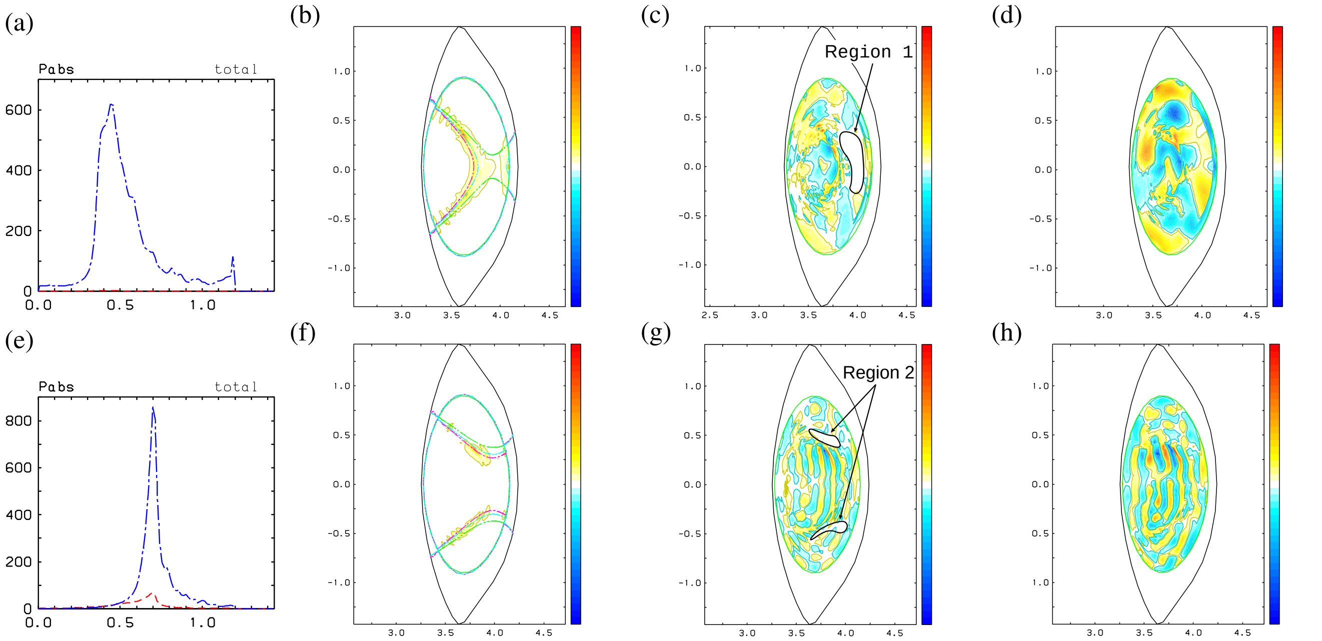

Fig. 4 Radial H absorption distributions (a), (e), contour plots of H absorption (b), (f), E_+ component (c), (g) and E_- component (d), (h) of the electric field on the poloidal cross section; LHD

Three lines drawn in Fig.4 (b), (f) represent ion cyclotron layer (a green line), two-ion-hybrid cut-off (a blue line) and resonance (a red line) layers from the outside. It is observed that the absorption region of minority ion locates near the minority ion cyclotron layer in Fig.4 (b), (f). These are the same tendency as that of tokamak plasma. But, it is not clear whether coherent waves are observed in the contour plots of the electric field on upper Fig.4 (c), (d). While, coherent waves is observed in lower Fig.4 (g), (h). In upper figures, the wave length is comparable to the plasma width. In lower figures,the wave length is shorter than the plasma width, because plasma dencity is higher. This is the reason for coherent waves observed. We observe that E_+ component of electric field is damped at region 1 and 2 in Fig.4 (c), (g) respectively. Region 1 and 2 locates at ion cyclotron layers. Region 1 is larger than ion cyclotron layer, because wave length is conparable to the plasma width.

4 Conclusions

We have studied the ICRF wave propagation and absorption in a 3D magnetic configuration using TASK/WM, in which Maxwell's equation for RF wave electric field is solved as a boundary value problem. The magnetic flux coordinates based on MHD equilibrium by VMEC code is considered. We have solved the wave propagation in the tokamak configuration (JT-60U) and in the helical configuration (LHD) in the minority ion heating regime.

The obtained results shows that ICRF wave is absorbed the region near the ion cyclotron layer and the two-ion-hybrid cut-off and resonance layer.

These analyses were carryed out under assumption of cold plasma. Not only the basic harmonics but also the second and higher harmonics are important. Therefore, we need to analyze including finite larmor effects. Furthermore, we need to analyze time evolution of velocity distribution function using GNET code.

[1] S. Murakami *et al* Nucl. Fusion 46 (2006) S425-S432.
[2] A. Fukuyama *et al Proc. 18th Int. Conf. Fusion Energy 2000* THP2-26.
[3] A. Fukuyama and T. Akutsu *Proc. 19th Int. Conf. on Fusion Energy 2002* THP3-14.